Advances in Cancer Prevention
ISSN: 2472-0429

Zahaf et al., Adv Cancer Prev 2016, 1:3
DOI: 10.4172/2472-0429.1000112

Research Article OMICS International

The Effect of the Posterior Loading on the Spine of a School Child

Samir Zahaf[1]*, Bensamine Mansouri[1], Abderrahmane Belarbi[1] and Zitouni Azari[2]

[1]Department of Mechanical Engineering, University of Sciences and Technology, Oran, Algeria
[2]Laboratory of Biomechanics, Polymers and Structures, ENIM-Metz, France

Abstract

The objective of this work is to study the effect of the backpack on the components of the spine system of a child school, know the effect of an eccentric force on the intervertebral discs, the creating a 3D model of the spine of a child of 38 kg overall weight under the effect of three eccentric load (P2, P3, P4) plus P1 compression load and calculated by the element method ends, For the boundary conditions we fixed the sacrum (Embedding the sacrum). We propose in this section to draw up a comprehensive study of the distributions of stresses and normal elastic strain of Von Mises in the intervertebral discs based on loads supported. The results show that the stress and strain of Von Mises are highest and concentrated in four intervertebral discs (D1, D2, D3 and D4), which causes a problem that calls (herniated disc). We concluded that the cause of the posterior load, a 300 mm lever arm with a 150 N force present maximum Von Mises stresses concentrated in four intervertebral discs (D1, D2, D3, D4), which justifies the distance between the load which is the point of application of the load and the axis of the spine plays a very important role in increasing the solicitation of the latter.

Keywords: Child; Herniated discs; Lumbar-thoracic; Intervertebral discs; Finite element; Biomechanics; Von Mises stress-strain; Disc degeneration

Introduction

Biomechanics is an important part of biology. Since 1978 there has been an enormous increase in scientific contributions from physicians and engineers. Recent basic study had been developed in many experiments and numerical analysis. In the last decade, more papers have been published in this area than ever before10 years old [1].

Lumbar disc herniation is defined as a more or less projection of the disc material (Figure 1) through a dehiscence of the fibrous ring, especially sitting at L4L5 or L5S1 [2]. Several terms have been used for designating this affection, especially by varying the degree of outsourcing the nucleus [3]. For a degenerated disc in flexion-compression, hernia corresponds to a migration (protrusion) posterior and especially posterolateral of the nucleus pulposus, pulling on the fibers of the anulus or bursting them, which extends towards the channel final spinal. The nucleus may outsource completely covered by the remaining ligament of the posterior annulus (prolapse appointed position) or may exceed this ligament and to project into the channel, becoming a "sequestered disc fragment." In all these situations the nervous structures can be compressed, generating low back pain or radiculalgia and important functional limitations [4]. The etiological factors are many: disc degeneration related to age, acute trauma, minor trauma but repeated [5-7], structural deficiencies of the annulus [8,9], biochemical factors or genetic, responsible for hereditary predisposition for herniated discs adult or juvenile Simmons'96; Matsui'98. More rarely, a rigid fusion can cause a hernia at adjacent [10].

Wearing a backpack too heavy (Figure 2) is certainly an aggravating factor and can cause long-term pain in the neck and shoulder, upper and lower back, pressure on the hips and knees and deformities of the spine, in biomechanics weight of the backpack is an eccentric posterior load applied to the lumbosacral spine, the weight should not exceed 10% of the weight of the child. It is between 8 and 15 years since the child's back is the most fragile, and scientific studies have demonstrated imaging (MRI) the risk of joint damage and intervertebral disc are real.

The diagram Figure 2 represents a school child to age 10 years of overall specific weight 38 kg to wear a backpack, backpack is the mass of 15 kg representing the weight P4.

The MRI study [11,12], alerts of this overweight effect in the development of degenerative disc disease, back pain and then herniated disc (Figure 3). In this work, the simulation of the disc degeneration, based on a finite element model of the spine depending on the mechanical properties were established; the boundary condition has been applied in the frontal plane to define restriction on movements of translation and rotation of the spine.

We propose in this work to draw up a comprehensive study of stresses and deformations in the spinal discs distributions based on supported loads. The results show that the level of degeneration increased in all intervertebral discs but concentrated in the four disks D1, D2, D3 and D4.

Figure 3 shows two vertebrae of the spinal column with an intervertebral disc under the effect of a compound loading (compression P1+bending moment P4). The compressive load P1 creates an internal pressure in the nucleus, this pressure will there after generate the disc degeneration or degenerative disc disease (Figure 4) as regards the forward flexion P4, if the load of the schoolbag increases, automatically distance between the point of load application and the axis of the spinal column increases, we see that the posterior portion of the annulus fibrosis is compressed and the other front portion is tensioned, that is to say the nucleus pulpous burst back (posterior compression), this compression produced by disc protrusion comes into contact with a nerve root called herniated disc.

***Corresponding author:** Samir Zahaf, Department of Mechanical Engineering, University of Sciences and Technology, Oran, Algeria, Tel: +213 (041) -56 03 27; E-mail: zahafsamir1983@gmail.com

Received July 27, 2016; **Accepted** August 18, 2016; **Published** August 26, 2016

Citation: Zahaf S, Mansouri B, Belarbi A, Azari Z (2016) The Effect of the Posterior Loading on the Spine of a School Child. Adv Cancer Prev 1: 112. doi: 10.4172/2472-0429.1000112

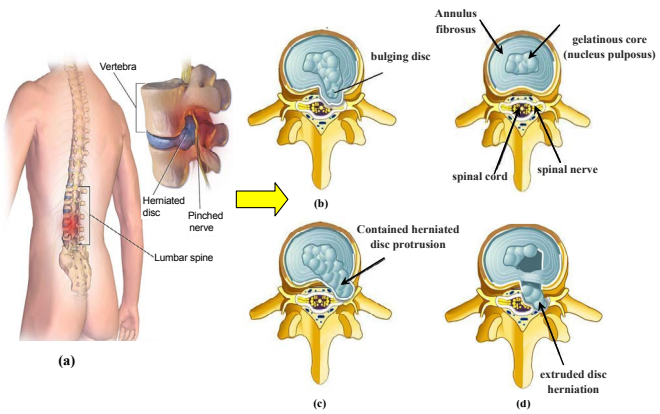

Figure 1: Evolutionary forms of the herniated disc. (a) constitution spine. (b) - crack the annulus, (c) -progression the disc material, (d) – prolapse [11] and www.espalda.org.

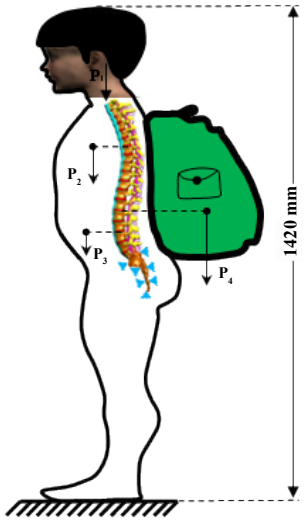

Figure 2: Constitution spine (school children) at the disc depending on its condition.

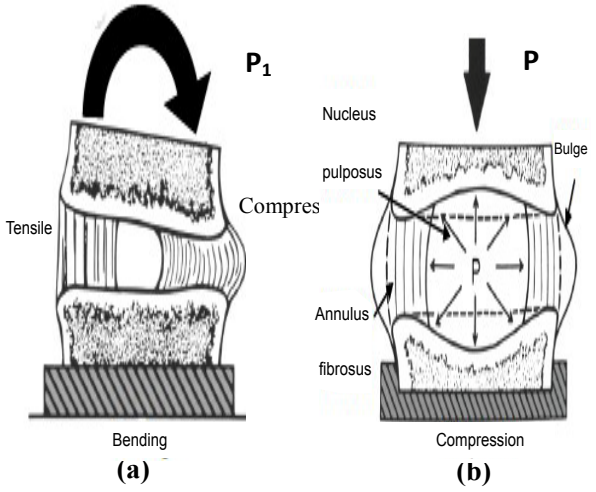

Figure 3: The intervertebral disc with (a) bending (b) compression [13].

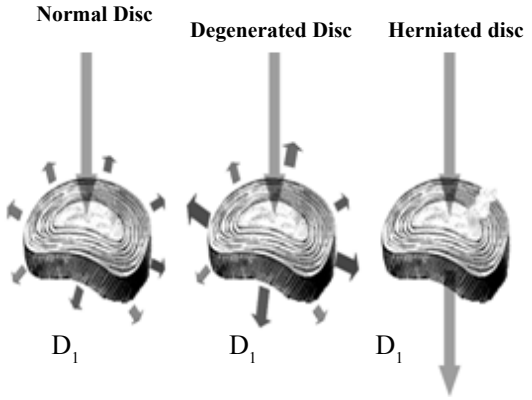

Figure 4: Load distribution at the disc D1 according to his state [14].

Material and Methods

The objective of this study was to investigate the effects induced by an eccentric load of the backpack on the back of a child, know the effect of an eccentric load on the intervertebral discs, created a 3D model of spine, the total mass of child is 38 kg under the effect of three eccentric loads (p2, p3, p4) plus a p1 compression load and calculated by the finit element method, the boundary conditions we fixed the sacrum (incorporation of the sacrum).

The analysis of biomechanical problems includes several steps.

The first is to study the form to define the geometrical configuration of the object, which allows the reconstitution of the vertebra, the ligament and bone using CAD programs.

The result is a 3D geometric model including these three components will then be prepared for use in finite element analyzes for the study of stresses and deformations distribution in the system.

The steps for the execution of the 3D vertebra model (Figure 5) are as follow:

a) Draw cortical bone that is the upper hinge and the lower hinge, then make the smoothing process; this gives a solid body called the vertebral body.

b) Secondly, draw the posterior arch (blade with the pedicle) with the spinous process.

c) Finally we draw the transverse process.

The simulation of the disc degeneration is based on a finite element model of the healthy spine. Figure 6 shows a spine model, this consists of five lumbar vertebrae (L1, L2, L3, L4 and L5) plus the sacrum, twelve thoracic vertebrae (TH1, TH2, TH3, TH4, TH5, TH6, TH7, TH8, TH9, TH10, TH11, TH12) and 17 inter vertebral discs between (S1-L5, L5-L4, L4-L3, L3-L2, L2-L1, L1-TH12 TH12-TH11, TH11, TH10, TH10-TH9, TH9-TH8, TH8-TH7, TH7-TH6, TH6-TH5, TH5-TH4, TH3-TH4, TH3-TH2 TH2-TH1) and various ligaments thoracic lumbar spine (anterior longitudinal ligament, posterior longitudinal ligament, ligament interspinous, ligament supraspinatus, yellow ligament and capsular ligament).

In static loading conditions, the model of the reconstructed spine is used in an analysis for studying the role of the inter vertebral discs and the stress distribution in these disks as well as its supporting structures.

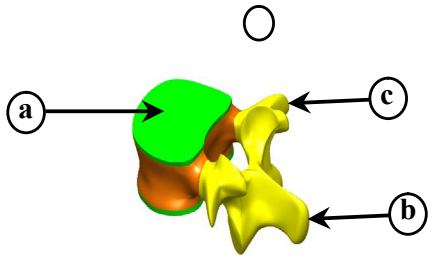

Figure 5: Lumbar vertebras.

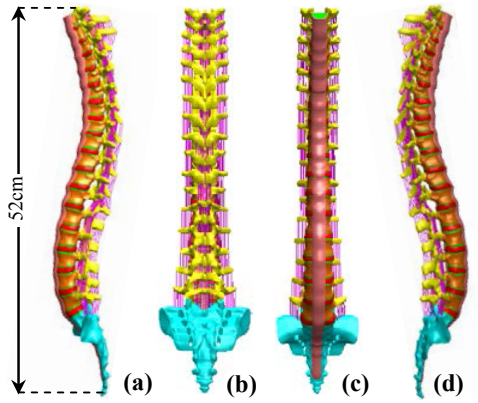

Figure 6: Spine studied. (a): Lateral (left) view. (b): dorsal view. (c): front view. (d): lateral (right) view.

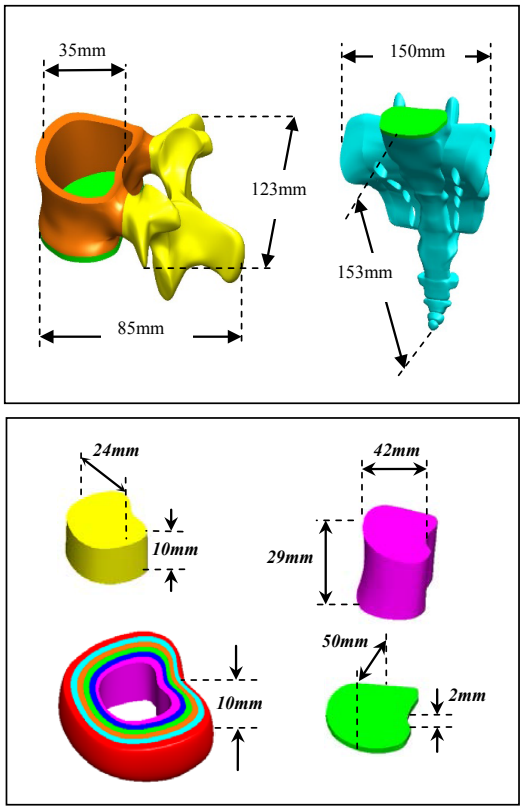

Figure 7: Vertebra and sacrum dimensions.

The spine is reconstructed in 3D to study the system dimensions (IVD - ligament-bone) (Figure 7).

In order to define the boundary conditions, restriction on movements of translation and rotation of the spine has been applied in the lower plane, and defined as having zero displacements. Several charges in the anterior direction were applied as follows:

- The application of the load on the upper side of the thoracic vertebra TH1.
- The fixed part applied to the body of the sacrum.
- The interfaces between the different components of the system of the spine, the cortical bone, the inter vertebral disk and ligament are treated as perfectly bonded interfaces (Figures 7 and 8).

Figure 9 shows an isometric view of an explored assembly of the spine and each component of the spine system is denoted by letters.

The selection of constitutive equations of the vertebral bone is defined as the part of the bone which carries the inter vertebral disc, composed of cortical bone, cancellous bone, the posterior arch, with a Young's modulus of about 12000 MPa. It is well known that cortical bone has better load capacity than the cancellous bone. Cortical bone is considered as an isotropic material, and homogeneous linear elastic (Table 1).

Table 1 shows the tensile strength of the structure annulus fibrosis according to different authors. These materials are anisotropic and non-linear elastic.

The behavior of inter-transverse ligament and inter-spinous ligament is nonlinear viscoelastic as in previous studies [13-16]; a linear elastic model is chosen to represent this behavior.

ANSYS WORKBENCH software was used for analyzing this geometry and generates the most suitable mesh. For the studied behavior, we used tetrahedral elements, type Solid187 conforming to defined parametric surfaces interfaces (Figure 10).

It is necessary to mesh the components of the spine with small and confused elements to ensure optimum accuracy of the results of stresses and strains in the inter vertebral discs.

The material properties of the spine components were selected after a careful review of the published literature (Table 2); it was considered appropriate to define the cortical and cancellous bone as homogeneous and isotropic. The magnitudes of 12000 MPa and 100 MPa (cortical and cancellous, respectively) were observed in all studies by various researchers.

Since physiologically the nucleus is fluid filled, the elements were assigned low stiffness values (1 MPa) and near incompressibility properties (Poisson's ratio of 0.499). Biologically, the annulus fibrosus is comprised of layers of collagen fibers, which attributes to its non-homogenous characteristics. However, due to limitations in modeling abilities, the annulus was defined as a homogenous structure with a magnitude of 4.2 MPa.

This was based on the modulus of the ground substance (4.2 MPa) and the collagen fibers reported in the literature, taking into account the volume fraction of each component. The complete model of the spine (Figure 10) was realized by the SOLIDWORKS SOFTWARE VERSION 2014 and was then transferred to the software Calculates

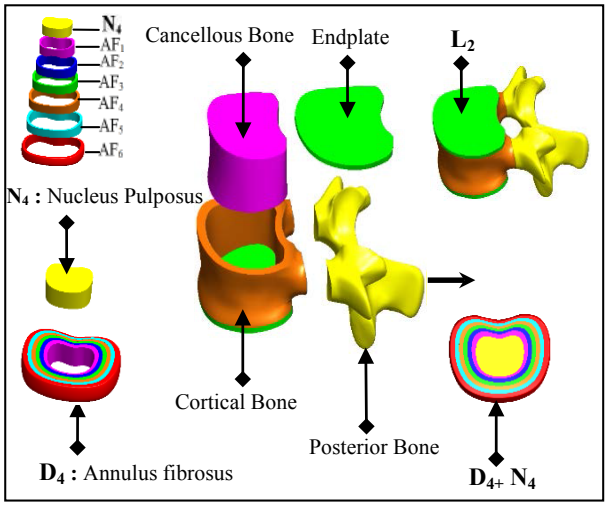

Abbreviations
D4: intervertebral disk upstairs four.
N4: nucleus in the intervertebral disc upstairs four.
D2: intervertebral disk upstairs two.
N2: nucleus in the intervertebral disc upstairs two.
L2: lumbar vertebra is on level two.
D4: intervertebral disk upstairs four.
N4: nucleus in the intervertebral disc upstairs four.
AF1: annulus fibrosus one.
AF2: annulus fibrosus two.
AF3: annulus fibrosus three.
AF4: annulus fibrosus four.
AF5: annulus fibrosus five.
AF6: annulus fibrosus sixe.
MRI: magnetic resonance imaging.
FEM: Finite Element Method.
IVD: inter vertebral disc.

Figure 8: 3D modeling thoracic vertebra L3, D4 disc of the lumbar spine (SOLIDWORKS 2014 software).

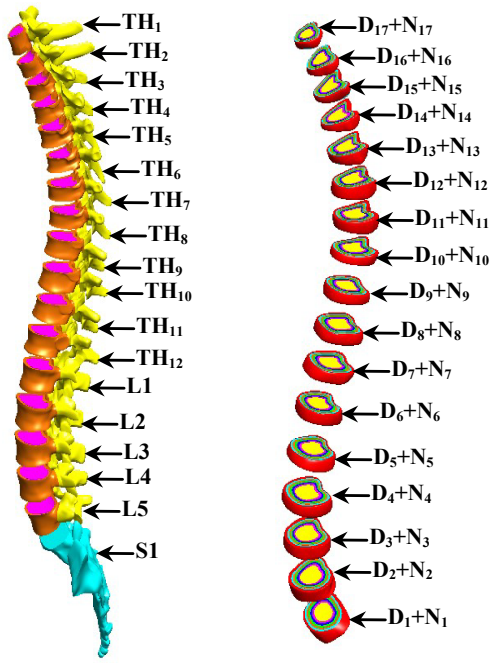

Figure 9: Assemblies in isometric perspective.

Authors	σ_r (MPa)
Brown (axial direction)	1.4
Galante (horizontal direction)	3.5 ± 0.3
Galante (fiber direction)	10.7 ± 0.9
Wu	3.7

Table 1: Mechanical characteristics of disc tissue [15].

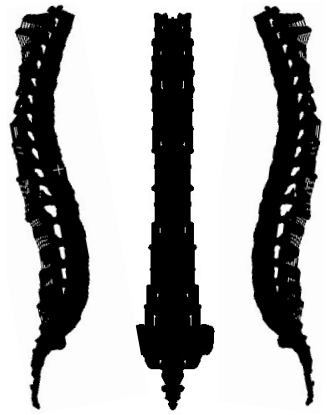

Figure 10: Spine 3D finite element modeling (ANSYS 14.5 software).

Material	Young modulus (MPa)	Poisson coefficient	References
Cortical Bone	12000	0.3	[17,19-28,33,42,44,45-47,49,50]
Cancellous Bone	100	0.2	[17,19-28,33,42,44,45-47,49,50]
Posterior Bone	3500	0.25	[19-21,24,25,27,28,30,33,34,43-46]
Cartilage Endplates	12000	0.3	[27,29,31,35]
Annulus Ground Substance	4.2	0.45	[17,20,23,25-29,31,33,37,38,41-46,49,50]
Nucleus Pulposus	1	0.499	[18,20-24,26,27,33,36,39,40-45,49,50]
Anterior Longitudinal Ligament	20	0.3	[20,21,23-25,43,44,47,48]
Posterior Longitudinal Ligament	20	0.3	[20,21,23,24,43,44,47,48]
Ligamentum Flavum	19.5	0.3	[20,21,23,24,43,44,47,48]
Intertransverse Ligament	58.7	0.3	[20,21,23,24,43,44,47,48]
Inter-Spinous Ligament	11.6	0.3	[20,21,23,24,43,44,47,48]
Supra-Spinous Ligament	15	0.3	[20,21,23,24,43,44,47,48]
Capsular Ligament	32.9	0.3	[20,21,23,24,43,44,47,48]

Table 2: Material Properties Specified in the Model.

each element ends ANSYS 14.5 WORKBENCHE generated the default mesh then generated linear global custom mesh tetrahedra 10 nodes conform to surface.

The three views of spine model with condensed mesh are shown in Figure 10. All element and node numbers are specified in Table 3.

Figure 10 shows a complete model that consists of 6053646

Component	Nodes	Elements	Thickness
Cortical Bone	724644	471775	1 mm
Cancellous Bone	454799	2377296	1 mm
Posterior Bone	3E+06	2377091	1 mm
Cartilage endplates	395500	234465	1 mm
Annulus Ground Substance	502860	244392	1 mm
Nucleus Pulposus	97864	63524	1 mm
Anterior Longitudinal Ligament	127791	74925	1 mm
Posterior Longitudinal Ligament	37241	19574	1 mm
Ligamentum Flavum	30226	13447	1 mm
Transverse Ligament	285328	131648	1 mm
Inter-Spinous Ligament	28968	13158	1 mm
Supra-Spinous Ligament	17833	8279	1 mm
Capsular ligament	51816	24072	1 mm
TOTAL	6E+06	6053646	1 mm

Table 3: Element and node numbers in the column vertebral system components.

elements and 6196007 nodes. Cortical bone contains (471775 elements and 724644 nodes), cancellous bone contains (2377296 elements 454799 nodes).

The posterior arch was modeled with tetrahedral elements to 10 nodes contains (2377091 elements, 3441137 nodes), the nucleus pulposus in the annulus fibrosus were modeled with tetrahedral type elements 10 nodes (63524 element 97864 nodes), the annulus fibrosus were modeled with elements of type tetrahedral to 10 nodes (244392 elements, 502860 nodes). The gelatinous cartilage modeled with a tetrahedral element to 10 nodes (234465 elements, 395500 nodes) [20-40].

Finally, the different types of ligaments generated by a tetrahedral mesh to 10 nodes (Table 3).

The diagram in Figure 11 represents a school child standing of 38 kg overall density, total mass (Head, Neck, Arm (left + right) Forearm (left + right) hand (left + right) is 6.9572 kg deviser by the upper surface of TH1 thoracic vertebra showing the pressure P1, P2 charge represents the mass of the body superior Trunk is 6.0648 kg, the distance between the load P2 is the point of application of the load and the axis (yy ‘) is 80 mm (Figure 11) [40-53].

The total mass of the lower trunk of the human body equals 10.45 kg represented by P3, the distance between the point of application of the load P3 and the axis (yy ‘) is 100 mm mm (Figure 11).

P4 load is the maximum weight of the backpack worn by the child (15 kg), the distance between the P4 specific weight that is the point of application of the load and the axis of the spine (300 mm) mm (Figure 11).

For the boundary conditions we fixed the sacrum (Embedding the sacrum) mm (Figure 11).

We propose in this section to draw up a comprehensive study of the distributions of the normal stresses of Von Mises and normal elastic strain of Von Mises in the intervertebral discs as a function of supported loads. Distributions of global stress state for each component of our model were presented in the posterior loading effect.

A quantitative analysis was performed based on a scale of progressive visual colors predefined by the software used (ANSYS Workbench 14.5), ranging from dark blue to red.

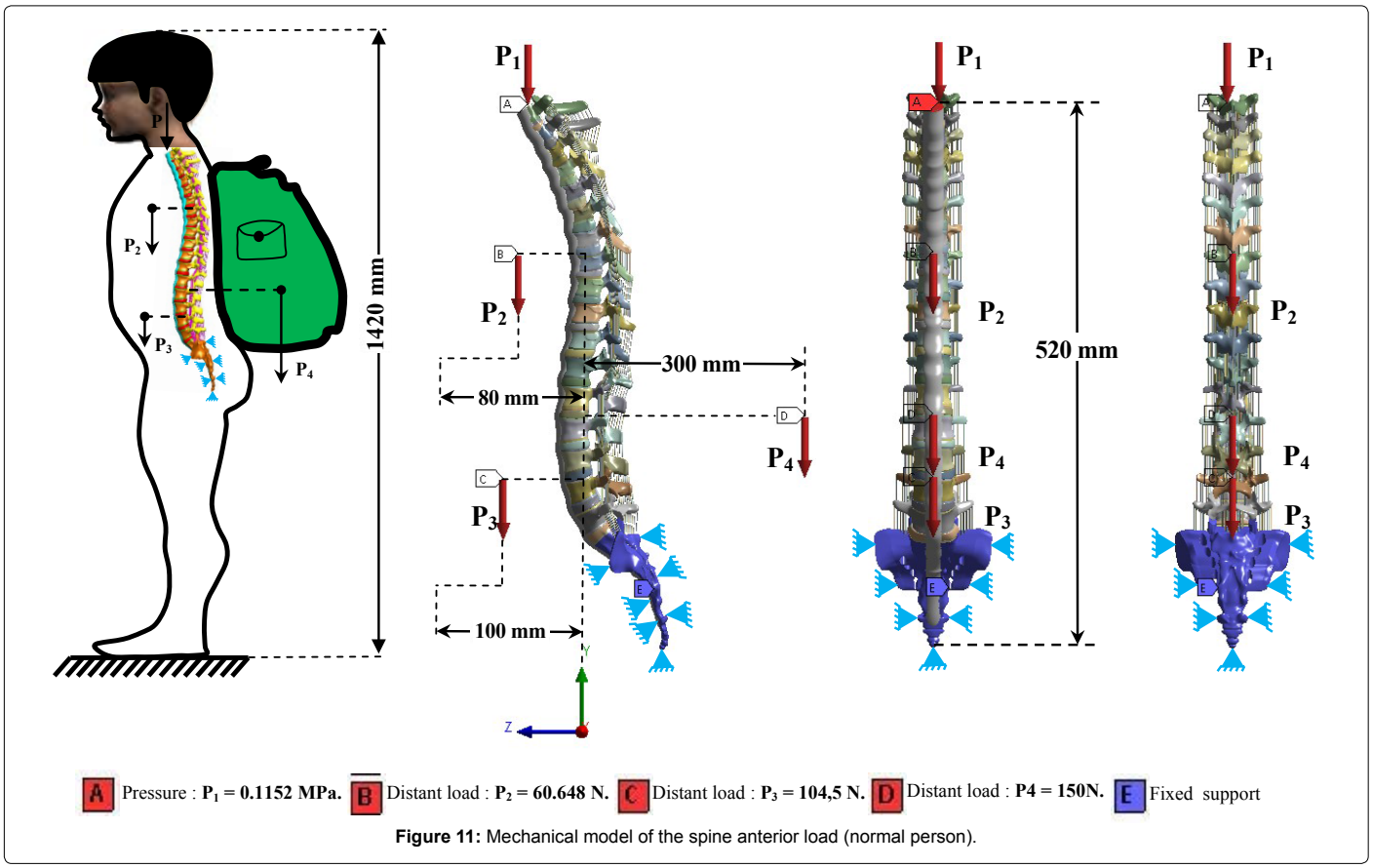

Figure 11: Mechanical model of the spine anterior load (normal person).

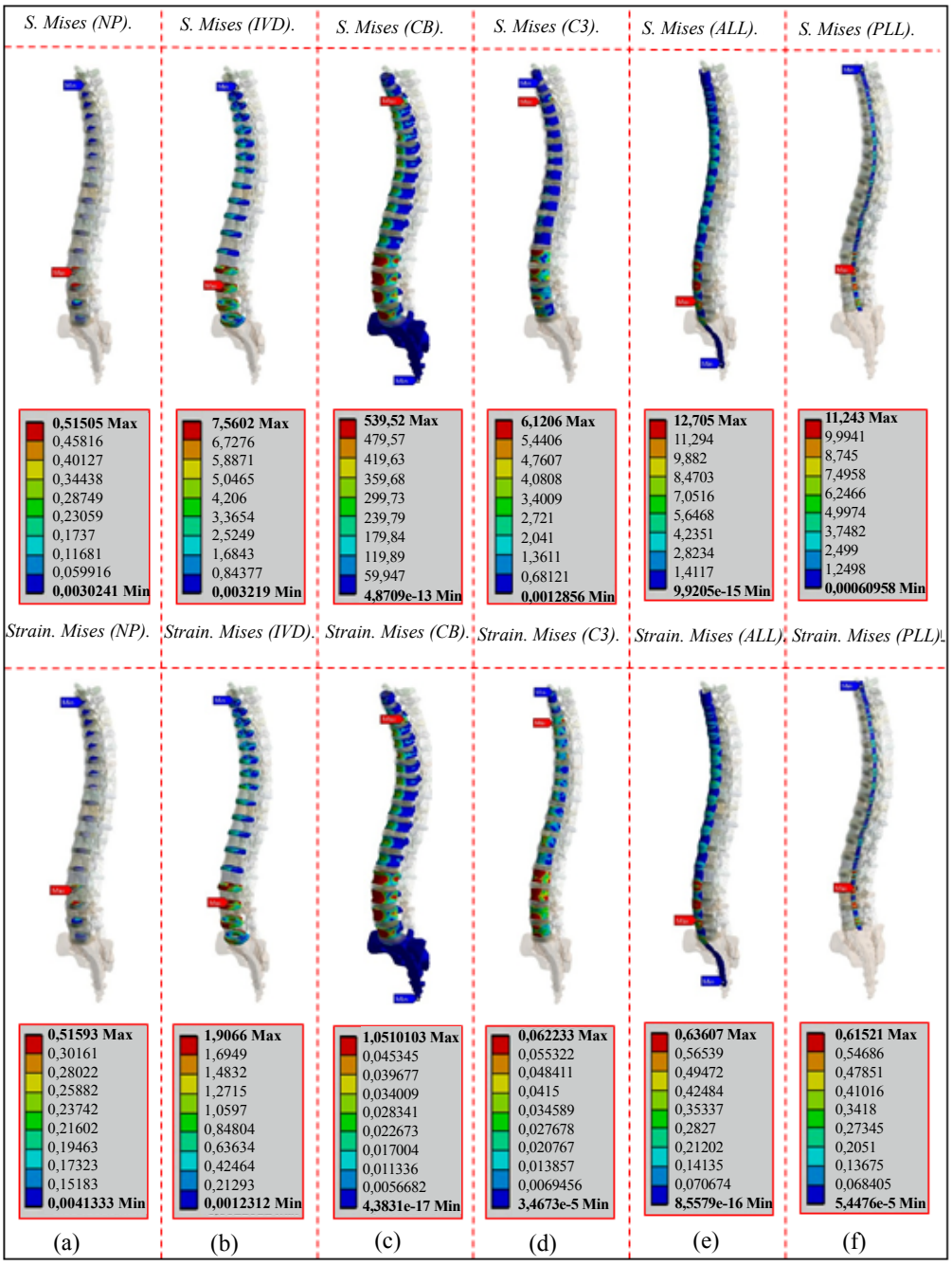

Figure 12: Distribution of the stresses and strains of Von Mises in the spine for a posterior load of 15 kg. (A) the nucleus pulposus, (b) the intervertebral disk, (c) the cortical bone, (d) the cancellous bone (e) anterior longitudinal ligament (f) posterior longitudinal ligament.

Results

We see in Figure 12 the stress distribution and strains Von Mises put in the components of the spine, we find that the posterior loading can cause long-term back pain and deformity of the spine. Figure 12 show a maximum value stress of Von Mises concentrated in the fourth intervertebral disk which are equal to 0.5150 MPa for the nucleus pulposus N4, 7.5682 MPa to the annulus fibrosis D4 and 539.52 MPa in the cortical bone of the vertebra thoracic TH3, 6.1206 MPa in the cancellous bone. A posterior loading shows that the distribution of the maximum Von stresses in the ligaments (anterior, posterior) concentrated at the back and equal to 12.705 MPa, 11.243 MPa (red part) (Figure 12). Regarding the strains of von Mises, we notice that the values are at a maximum in the fourth intervertebral disc which is equal to 0.5159 mm/mm for the nucleus N4, 1.9066 mm/mm for the annulus fibrosus D4 compared by the other discs of the spine (red part) (Figure 12). The posterior loading of 15 kg to the back indicated that the maximum strain of von Mises concentrated in the components of the thoracic vertebra TH3, 0.051013 mm/mm for cortical bone, and 0.06223 mm/mm for cancellous bone this mentioned in the Figure 12. We notice in Figure 12 that maximum strains legends of Von Mises in

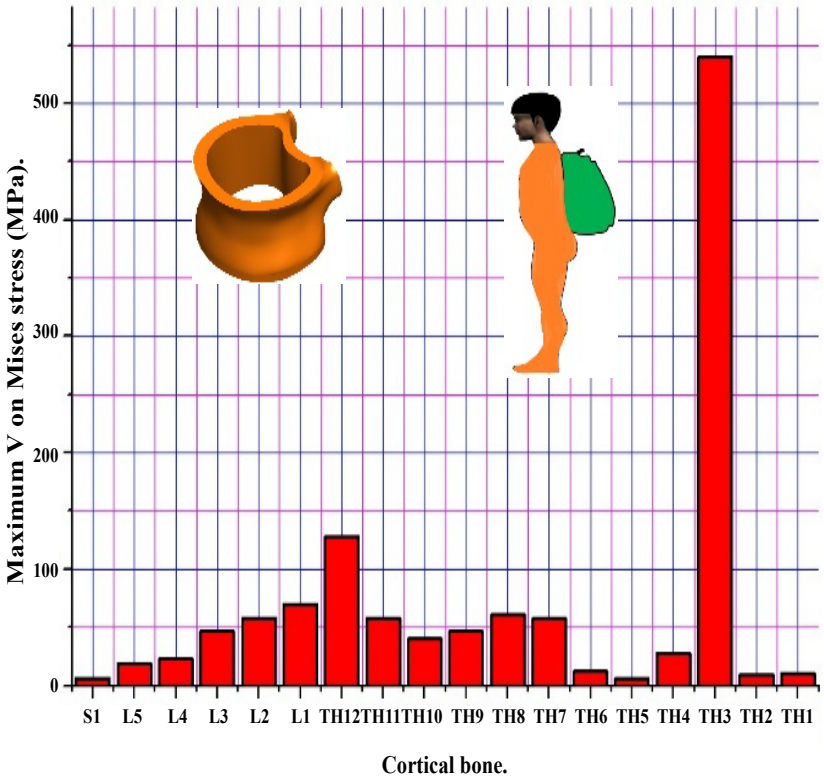

Figure 13: Histogram of Von Mises stresses in the cortical bone for posterior loading of 15 kg.

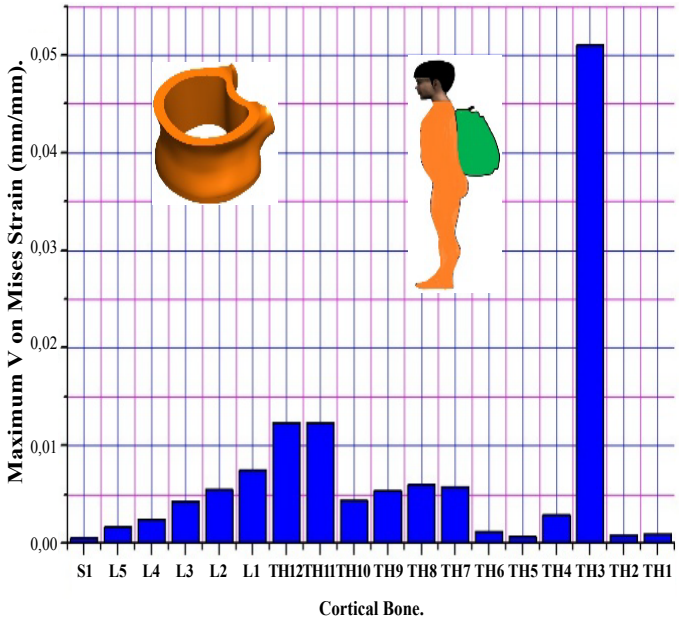

Figure 14: Histogram of Von Mises strains in the cortical bone for posterior loading of 15 kg.

the two ligaments (LLA, LLP) are equal to 0.63607 mm/mm, 0.61521 mm/mm (red part).

Figure 13 shows a histogram of the Von Mises stress put in the cortical bone, for a posterior load 15 kg, we find that the stress value concentrated in the six lumbar vertebrae L5, L4, L3, L2, L1, TH12, which are equal to 18,916 MPa, 23 168 MPa 46 552 MPa 58 405 MPa, 69.90 MPa, 128.29 MPa this mentioned in figure regarding that the stress of Von Mises will decrease from value of the cortical bone vertebra TH12 and increased up to 539.52 MPa which lie in the anterior and posterior part of the cortical bone TH3 (red part) (Figure 13).

Figure 14 shows a histogram of von Mises strain in the cortical bone reached a maximum value concentrated in six vertebrae L5, L4, L3, L2, L1, TH12, which are equal to 0.001617 mm/mm 0.0024 mm/mm 0.0042 mm/mm 0.0054 mm/mm 0.0074 mm/mm 0.01228 mm/mm, this mentioned in Figure 15 follows regarding the strains of von mises will decrease from the value of cortical bone of the vertebra TH11 and increased up to 0.05110 mm/mm which lie in the anterior and posterior part of the cortical bone TH3 (red part) (Figure 15).

We see in Figure 16 the Von Mises stresses a maximum value concentrated in three cancellous bone TH12, TH6, TH3 are equal to 1.3019 MPa 2.899 MPa, 6.1206 MPa for a lifted load of 15 kg which are located in the anterior and posterior part of the cancellous bone (red area) (Figures 17 and 18).

As regards the Von Mises strains (Figure 17) we notice that the values are maximal in the three cancellous bone TH12, TH6, TH3

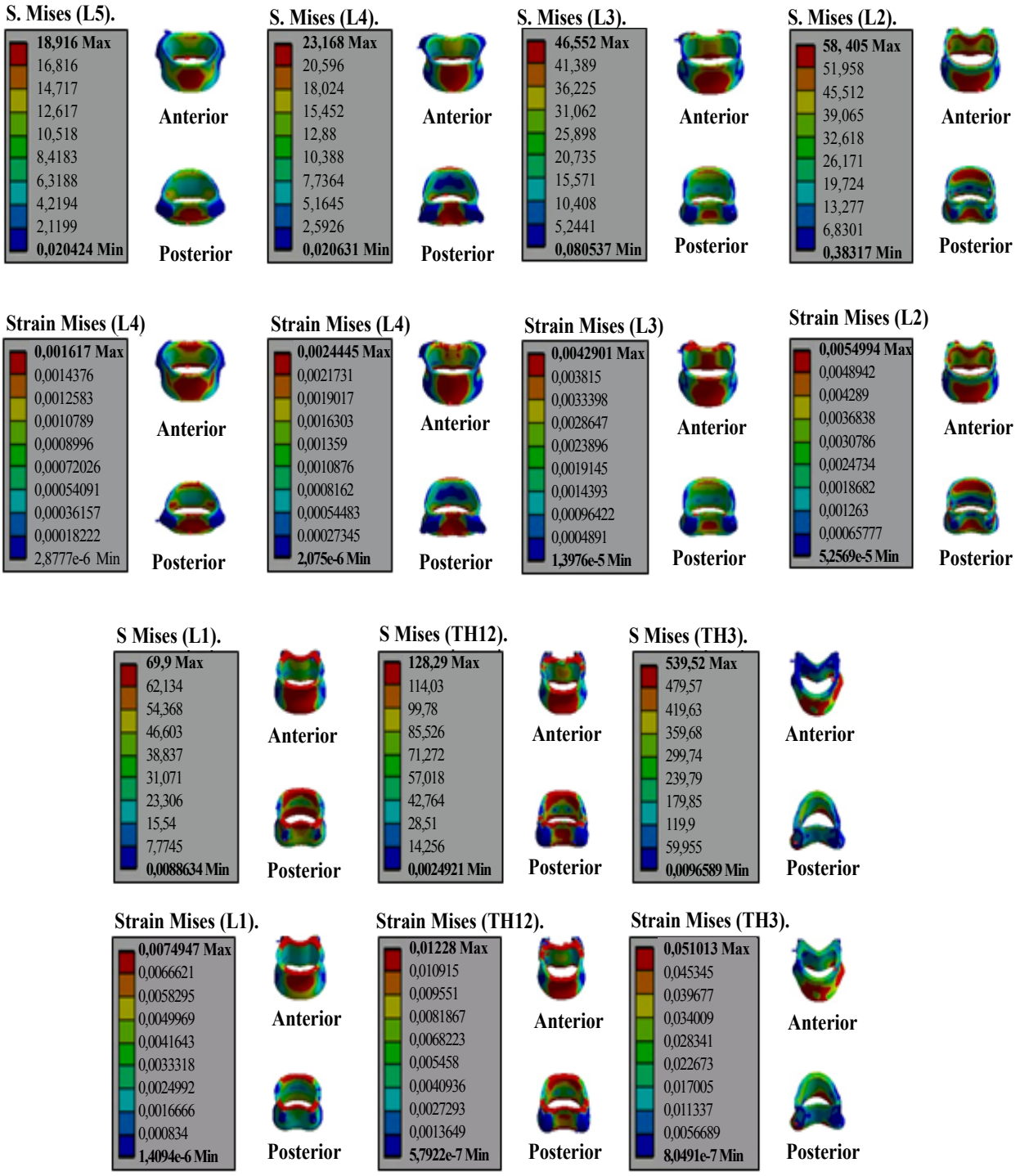

Figure 15: Distribution des contraintes et déformations de Von Mises dans l'os cortical pour un chargement postérieur de 15 kg.

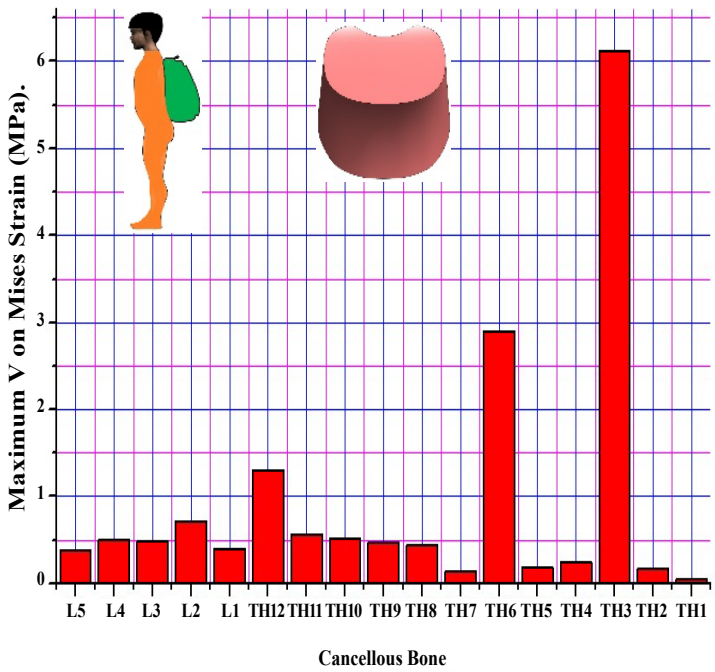

Figure 16: Histogram of Von Mises stresses in cancellous bone for posterior loading of 15 kg.

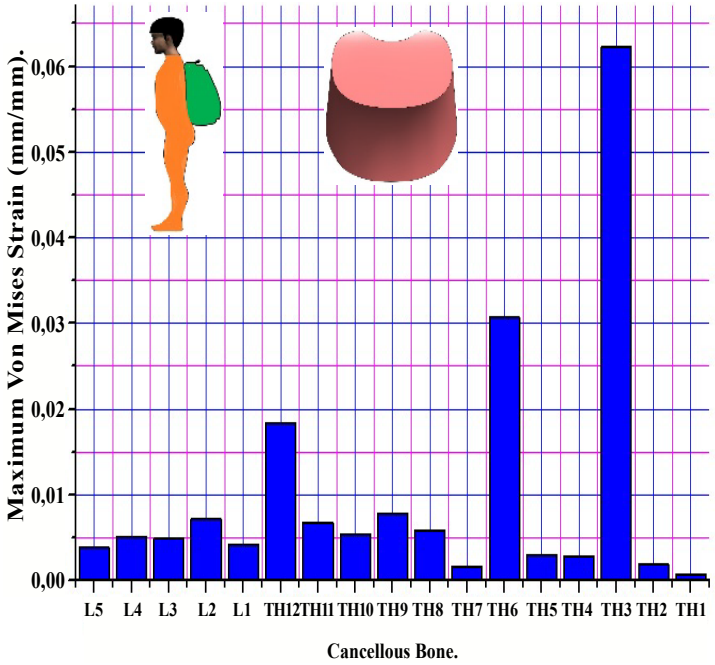

Figure 17: Histogram of Von Mises strains in cancellous bone for posterior loading of 15 kg.

0.0182 mm / mm, 0.03068 mm / mm 0.06223 mm / mm for a posterior load of 15 kg from the other components of the spine (red part) (Figure 18).

Figure 19 shows, schematically, the increase von Mises stresses in the intervertebral discs. On the one hand before a child carry a school bag 15 kg, 30 cm by the input axis (yy ') of the spine (30 cm behind the center of the intervertebral disc calculating the Von Mises stresses in intervertebral discs). We note in Figure 19 that the lifting of the load behind the abdomen the Von Mises stresses increased in the dorsal region that is to say the four intervertebral discs (D1, D2, D3, D4) are the most requested and are equal to (3.1168 MPa, 3.1615 MPa, 7.5682 MPa, 6.6882 MPa) mentioned in Figures 20 and 21.

Figure 19 shows, schematically, the increase von Mises stresses in the intervertebral discs. On the one hand before a school child carry a school bag 15 kg, 30 cm by the input axis (yy ') of the spine (30 cm behind the center of the intervertebral disc calculating the Von Mises

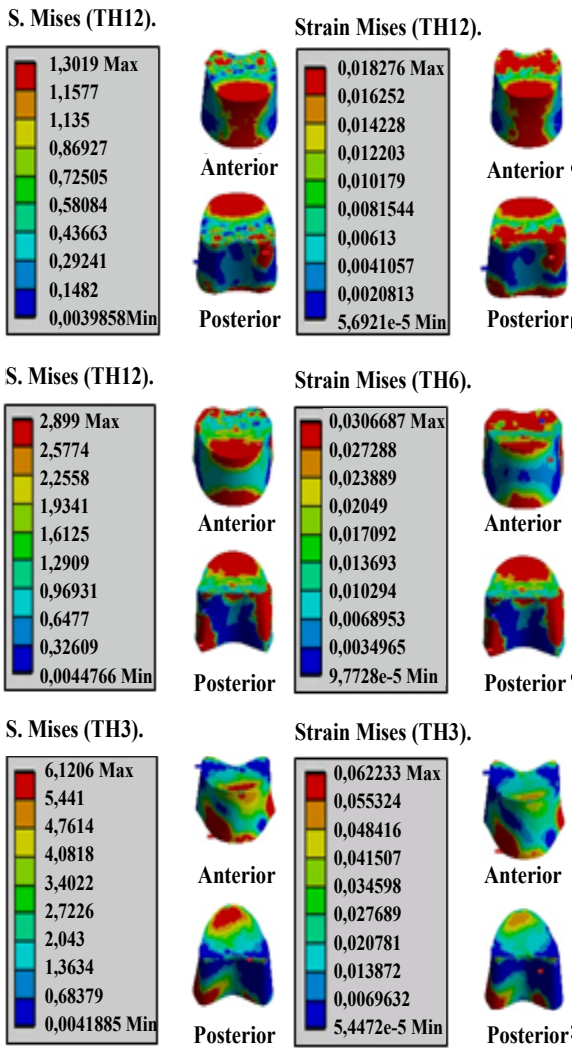

Figure 18: Distribution of the stresses and strains of Von Mises in the cancellous bone for a posterior loading of 15 kg.

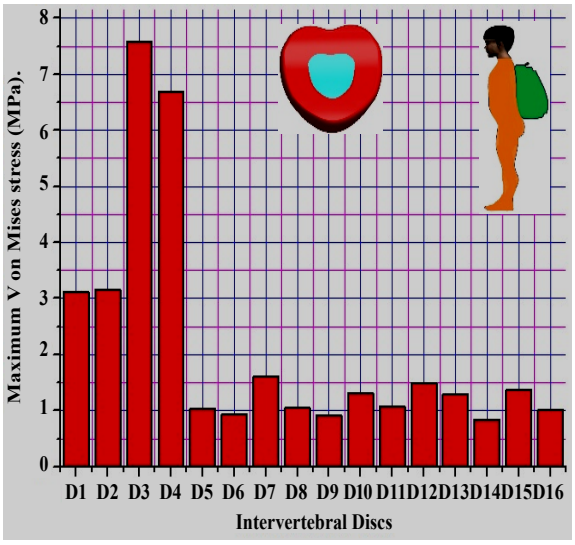

Figure 19: Histogram of Von Mises stresses in the DIV for posterior loading of 15 kg.

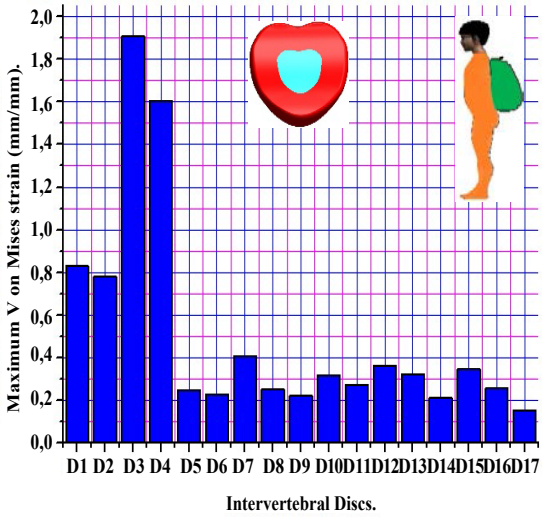

Figure 20: Histogram of Von Mises strains in the DIV for posterior loading of 15 kg.

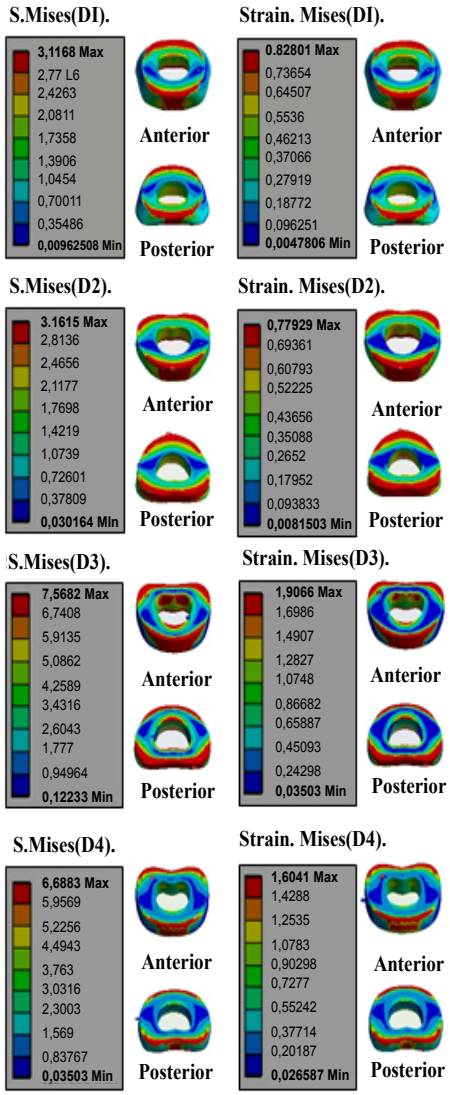

Figure 21: Distribution of the stress and strain of Von Mises in DIV (D1, D12, D3, D4) for posterior loading of 15 kg.

stresses in intervertebral discs). we note in Figure 19 that the lifting of the load behind the abdomen the Von Mises stresses increased in the dorsal region that is to say the four intervertebral discs (D1, D2, D3, D4) are the most requested and are equal to (3.1168 MPa, 3.1615 MPa, 7.5682 MPa, 6.6882 MPa) mentioned in this Figure 21.

The posterior load (load attached to the back) showing the maximum strain of von Mises concentrated in the four intervertebral discs (D1, D2, D3, D4) which are equal to (0.82801 mm/mm 0.7792 mm/mm 1.9066 mm/mm, 1.6041 mm/mm) this is mentioned in the Figures 20 and 21. We see in Figure 21 Disc degeneration begins, after an asymptomatic phase dehydration of two intervertebral discs (D3, D4) by tearing of the annulus fibrosus (AF6, AF5, AF4, AF3, AF2, AF1). The two core (N3, N4) can then migrate into the thickness of the ring and cause acute or chronic back pain. If it moves more through the ring, the two core (N3, N4) can protrude to the rear side of the disc while forming a HERNIATED DISC. This hernia can migrate into the spinal canal and even exclude leaving the disc. This disc herniation can come compressed or "pinched" to one or more nerve roots in the vicinity of the disc.

Figure 22 shows MRI of the spine in sagittal section in a boy of 12, we notice a stepped disc protrusion at L5-S1, L5-L4, L4-L3 under the posterior loading effect.

Figure 23 indicate a sagittal section of lumbar MRI, T2 showing the appearance of a herniated disc L4-L5 excluded associated with discale progression L3-L4 and S1--L5 under the posterior loading effect.

In standing position with a 15 kg load on the back of level we notice that the stress von Mises are maximum in the nucleus pulposus (N1, N2, N3, N4) and are equal to (0.3082 MPa, 0.313 MPa, 0.4869 MPa, 0.5150 MPa) (Figures 24 and 25).

Figure 25 shows the distribution of Von strains supported by the nucleus pulposus (N1, N2, N3, N4) and notes that the strain value is maximum in the two nucleus pulposus (N3, N4) by supplying the other systems of the spine (Figures 24-26).

The posterior loading shows suffering on the back level, Figure 27 shows a sagittal section of an MRI lumbosacral T2 showing disc degeneration (discopathy) at (S1-L5, L5-L4 and L4-L3) (a), (b) disc herniation (S1-L5) posterolateral right follows, we note in Figure 27

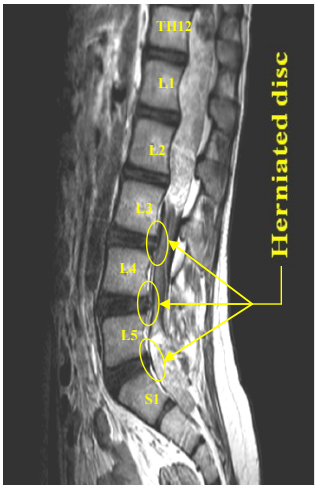

Figure 22: Lumbar MRI sagittal section in a boy of 12, T2-weighted sequence showing a stepped disc protrusion at L5-S1, L5-L4, L4-L3 [44].

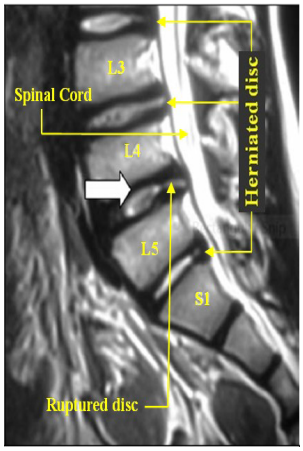

Figure 23: Sagittal section of lumbar MRI T2 showing the appearance of a herniated disc L4-L5 associated with discale progression L3-L4 and S1-L5 [45].

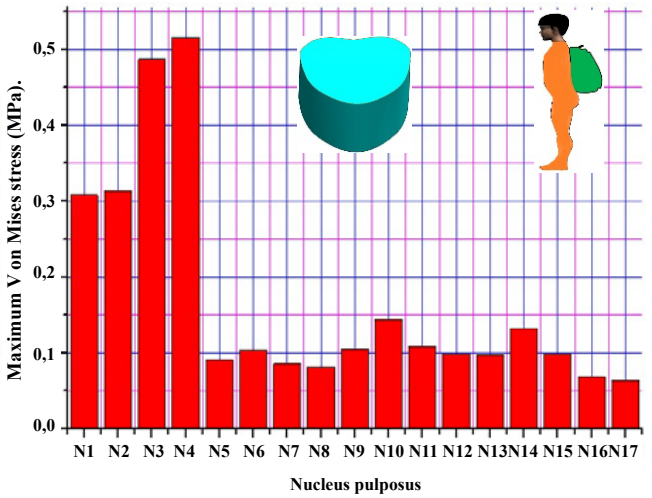

Figure 24: Histogram of Von Mises stresses in the nucleus pulposus (N1, N2, N3, N4) for posterior loading of 15 kg.

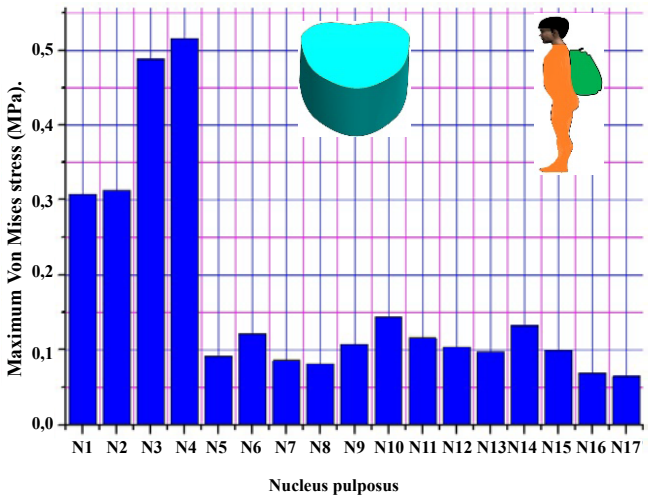

Figure 25: Histogram of Von Mises strains in the nucleus pulposus (N1, N2, N3, N4) for posterior loading of 15 kg.

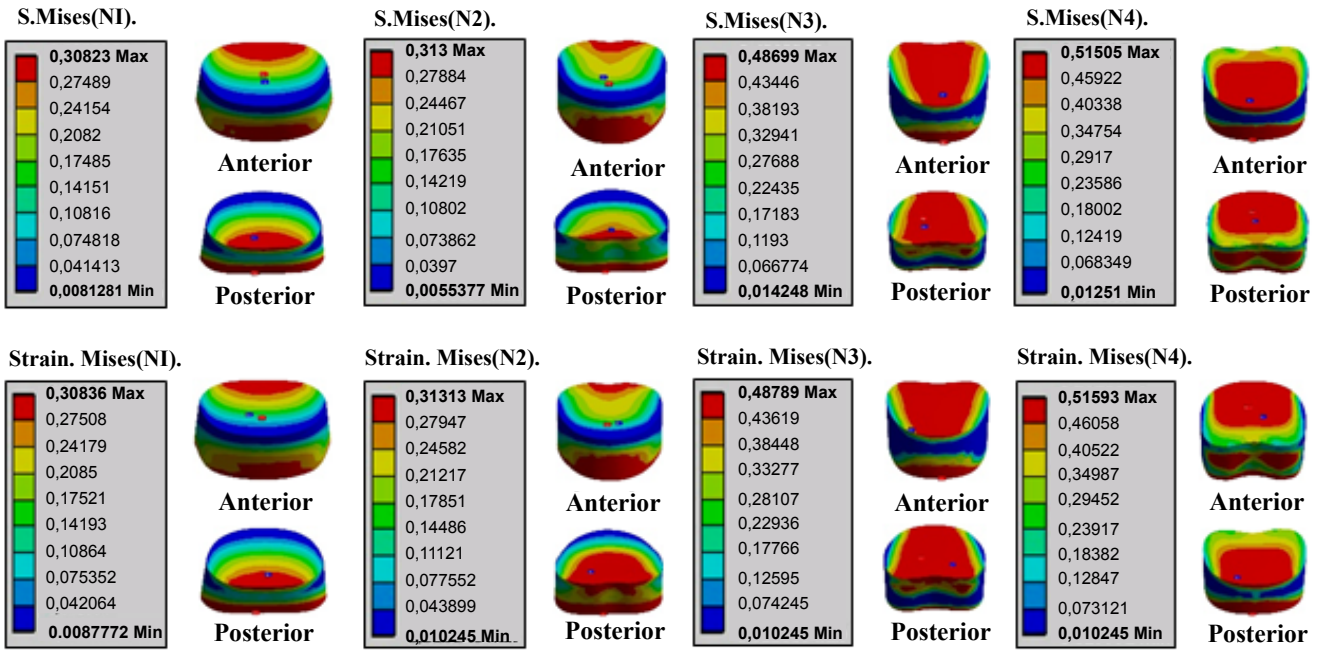

Figure 26: Distribution of the stresses and strains of Von Mises in nucleus pulposus (N1, N2, N3, N4) for a posterior loading of 15 kg.

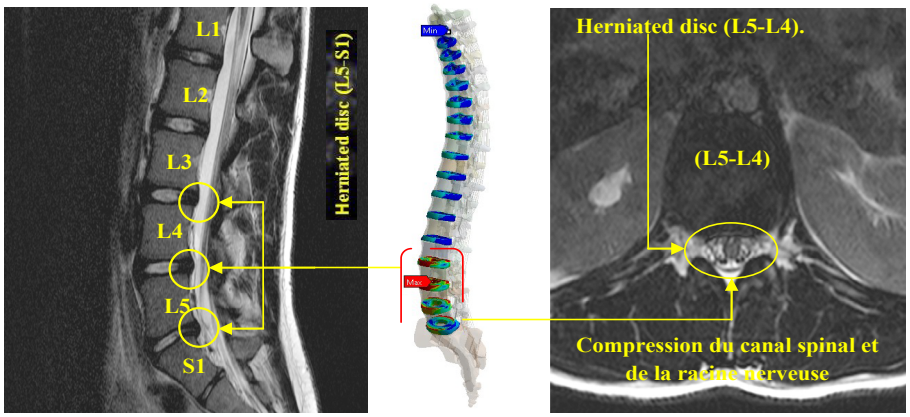

Figure 27: Sagittal section a lumbosacral MRI T2 showing disc degeneration (disc disease) at the level of (S1-L5, L5-L4 and L4-L3) (a), (b), showing a herniated disc (S1 -L5) posterior right lateral [46].

that the displacement of the central part of the two intervertebral discs (D1, D2) to the Exterior degenerative disc disease, and a traumatism / or more microtrauma can alter the two intervertebral disks and cause a tearing of the latter.

The two cores (N1, N2) moving can come compresses the spinal cord or a nerve root generating symptoms radiculopathy (Figures 27-29) above shows the stress distribution of Von Mises in the intervertebral disk (D3) and we see that disc degeneration starts, after a phase of asymptomatic dehydration, with tears in the annulus fibrosus (AF5, AF6).

The core (N3) can then migrate into the thickness of the annulus and cause acute or chronic back pain. If it moves further through the annulus, the core (N3) may protrude to the posterior face of the disc so forming a disc herniation. This hernia can migrate into the spinal canal and even exclude leaving the disc. This disc herniation can come compress or "stuck" in one or more nerve roots located near the disc.

The Von Mises stresses in the fibrous rings (N3, AF1, AF2, AF3, AF4, AF5, AF6) are equal to (0.4869 MPa, 1.8381 MPa, 2.2456 MPa, 2.82 MPa, 3.6215 MPa, 7.5682 MPa, 7.473 MPa) by report the other system components of the spine (Figure 29).

Figure 28 shows a histogram of maximum Von Mises stress in the disc of fibrous rings D3 (N3, AF1, AF2, AF3, AF4, AF5, AF6), we note that the nucleus pulposus (N3) starts move to outside that is tearing commenced by the fibrous rings (AF6) (AF5), AF4, AF3, AF2, AF1, the core (N3) can come compress the spinal cord or multiple roots or the dural sheath.

Figure 30 shows the histogram of Von Mises strains in the intervertebral disc components (D3) for a posterior load of 15 kg,

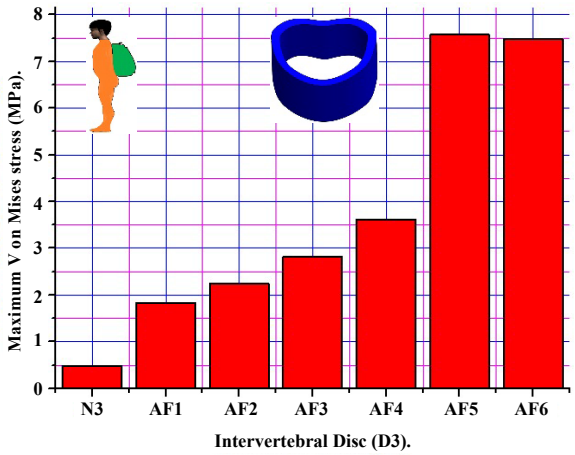

Figure 28: Histogram of Von Mises stresses in the DIV D3 for posterior laoding of 15 Kg.

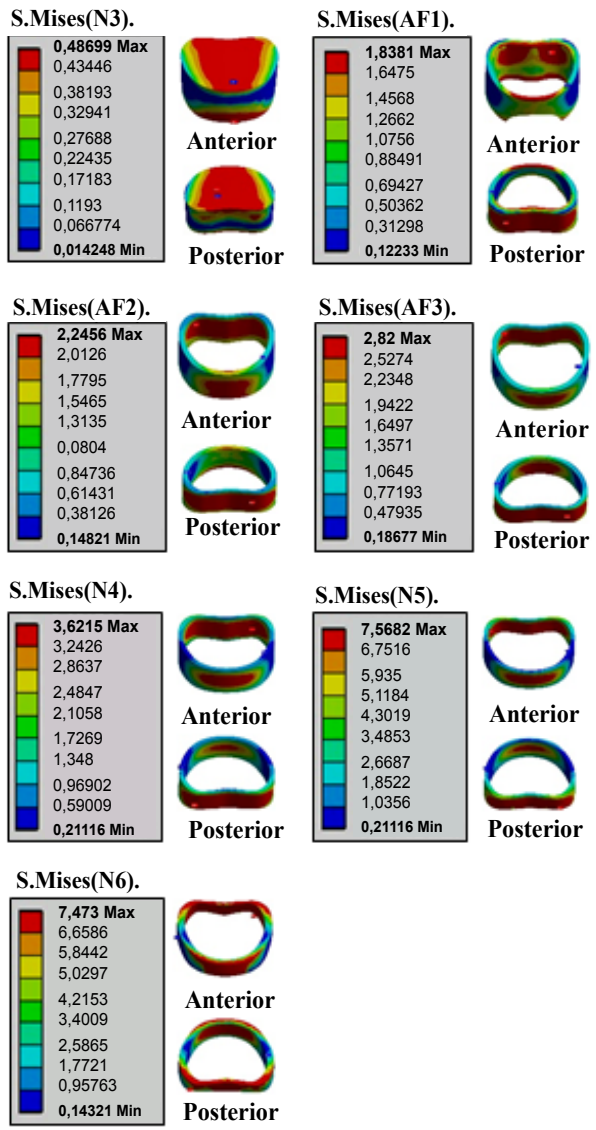

Figure 29: Distribution of Von Mises stresses in the annulus fibrosis (D3) for posterior laoding of 15 kg.

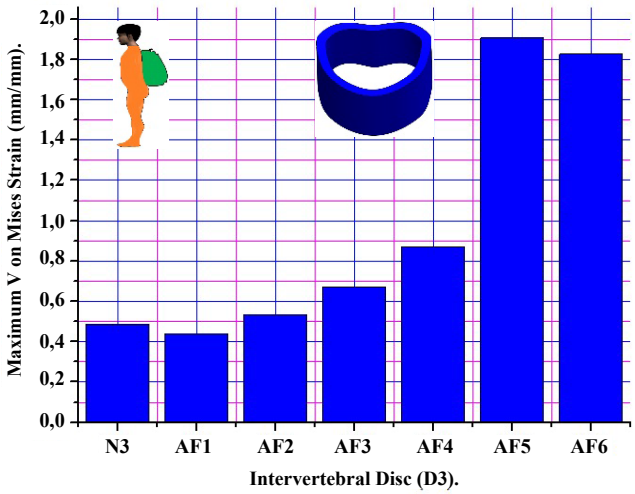

Figure 30: Histogram of Von Mises strains in the DIV D3 for posterior laoding of 15 Kg.

we note that the maximum von Mises strain are concentrated in the two rings (AF5, AF6) are equal to (1.9066 mm/mm 1.8265 mm/mm) and say this disc degeneration starts, after a phase of asymptomatic dehydration by tears to two the annulus (AF5, AF6).

In Figure 31 the posterior loading shows maximum von mises strains concentrated in the disc D3 (N3, AF1, AF2, AF3 AF4, AF5, AF6) and are equal to (0.4878 mm/mm 0.4377 mm/mm 0.5347 mm/mm 0.6724 mm/mm 0.8707 mm/mm 1.9066 mm/mm 1.8265 mm/mm) according the other systems of the spine.

Figure 32 shows the distribution of Von Mises strains in the disk fibrosus rings (D4) under the effect of a load composed (compression P1 plus bending moment (P2, P3, P4)), the load axial compression P1 on the upper surface of the cores (N4) creates a radial inner pressure at fibrosus rings D4 disc, the pressure by the following will generated disc degeneration (discopathy), as regards the anterior bending (P2, P3, P4) causes repetitive movements, if the posterior augment load, we notice the posterior part of each S.Mises (AF1). Anterior Posterior S.Mises (N3). Anterior Posterior Anterior Posterior S.Mises (AF2). S.Mises (AF3). Anterior Posterior S.Mises (AF4). Posterior Anterior S.Mises (AF 6). Anterior Posterior Anterior S.Mises (AF 5). Posterior ring fibrosis compress part in red and the other former party tender that is to say six gelatinous cores (AF1, AF2, AF3, AF4, AF5, AF6) stormed back (posterior compression), the (compression P1 produced by disc protrusion comes into contact with a nerve root called herniated disc.

A posterior load applied on the upper surface of the thoracic vertebra TH1 of the spine resulting in a maximum concentration of normal stresses in the anterior and posterior of the disk D4 (the red part) this is mentioned in Figures 33 and 34.

Figure 35 shows that the posterior loading presents a greater strain in the intervertebral disc D4, which means that the said disc is the most sought as posterior flexion thus thereby, it is noted in the Figure 35 that the towed part of the disc D4 is greater than the compressed portion (crushed).

We see in Figures 32 and 34 the Von Mises stresses affected a maximum value concentrated in the gelatinous core N3 with the rings fibrosis (AF1, AF2, AF3, AF4, AF5, AF6) of the disc intervertebral (D4) that are equal to 0.5150 MPa, 1.8824 MPa, 2.2162 MPa, 2.5111 MPa,

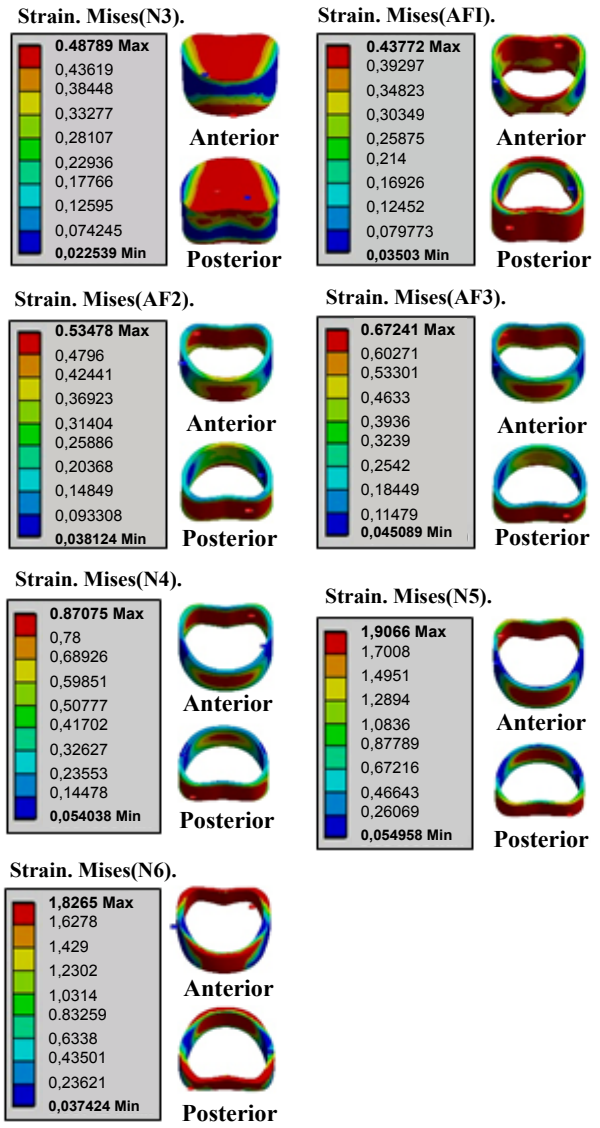

Figure 31: Distribution of Von Mises strains in the annulus fibrosis (D3) for posterior loading of 15 kg.

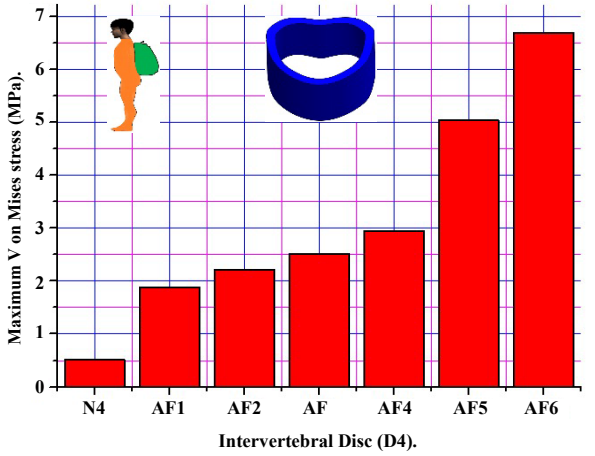

Figure 32: Histogram of Von Mises stresses in the D4 DIV for posterior loading of 15 Kg.

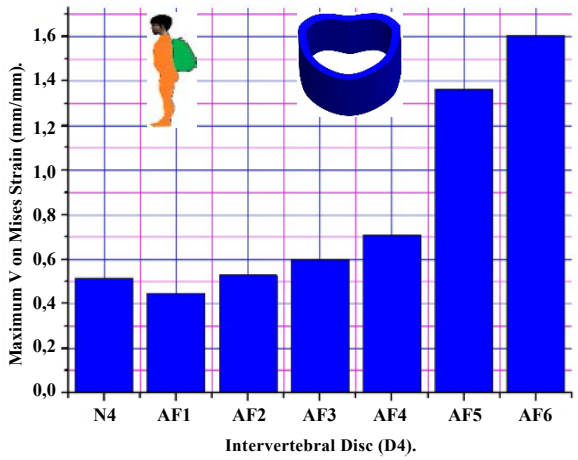

Figure 33: Histogram of Von Mises strains in the D4 DIV for posterior loading of 15 Kg.

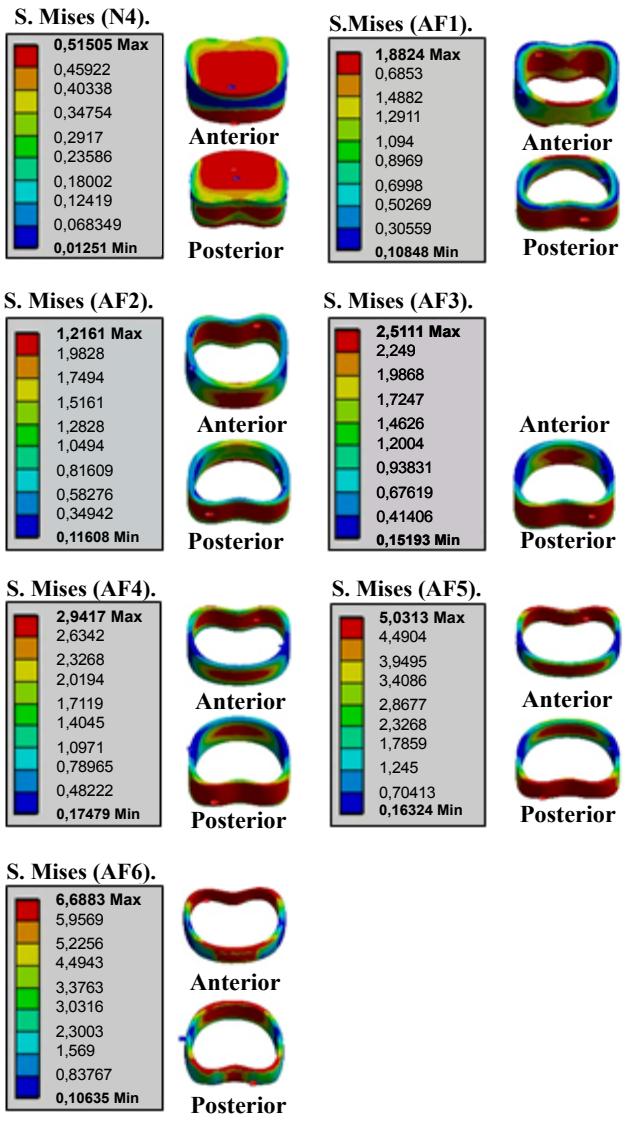

Figure 34: Distribution of Von Mises stresses in the annulus fibrosis (D4) for posterior loading of 15 kg.

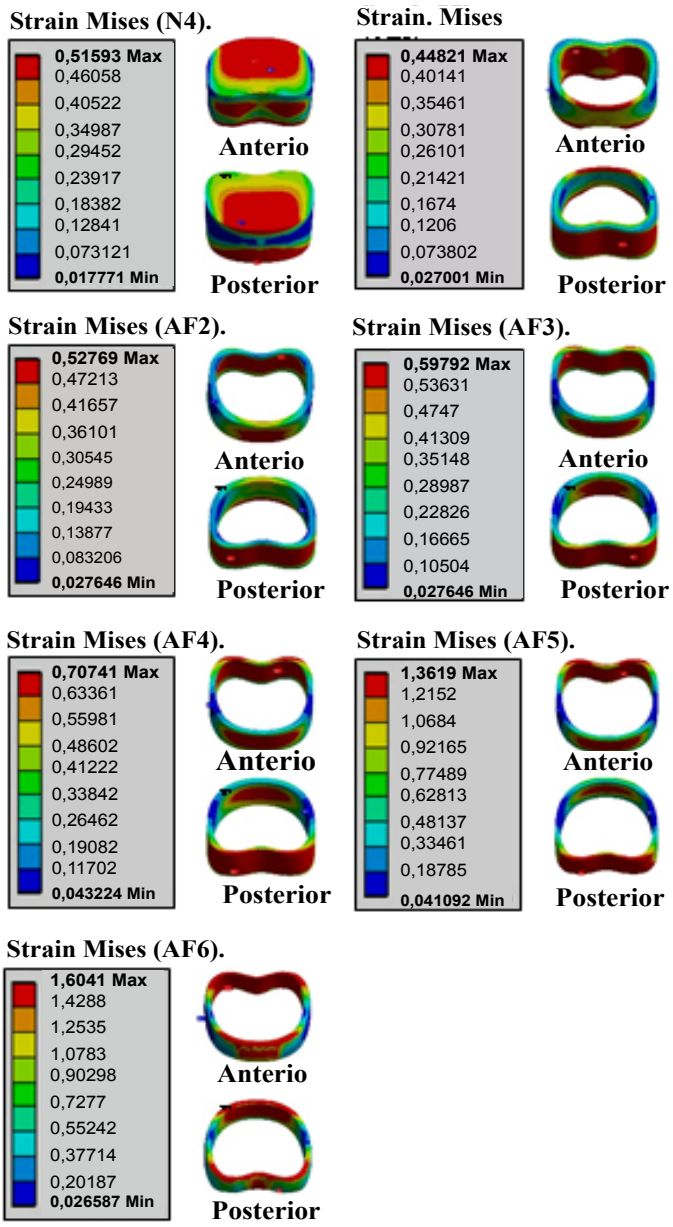

Figure 35: Images of a girl 14 years with back pain so grave she was unable to walk. lumbosacral spine radiographs of the posterior face (a) and lateral (b) show one great fault to extradural (L5-S1) (black arrow) which blocks almost completely the spinal canal to decrease the space between (L5-S1 and L5-L4), (c) TDM lumbosacral spine in axial section showing a herniated disc median (L5-S1) [47].

2.9417 MPa, 5.0313 MPa, 6.6883 MPa) for a posterior load of 15 kg which are in the anterior part and posterior of the intervertebral disk (red part).

The posterior loading shows that the von Mises strain value in the components of intervertebral disc D3 are maximum in the two last annulus fibrosus (AF5, AF6) (Figure 34).

On the other hand, the Figure 35 show the contour of the von Mises strains in the annulus fibrosus of the disk (D4) are equal (0.5159 mm/mm 0.4482 mm/mm 0.5276 mm/mm 0.5979 mm/mm 0.7074 mm/mm 1.3613 mm/mm 1.6041 mm/mm) according to the other system components of the spine.

Discussion

In sum, we concluded that wearing too heavy schoolbag 15 kg is certainly an aggravating factor, and may cause a long-term back problems and deformations of the spine, the 3D model of the spine of a child under the effect of an eccentric load and calculate by the FEM provokes stress and strains maximum of Von Mises concentrated in the four intervertebral discs (D1, D2, D3, D4) and are equal to (3.1168 MPa, 3.1615 MPa, 7.5682 MPa, 6.6882 MPa) (0.82801 mm/mm 0.7792 mm/mm 1.9066 mm/mm 1.6041 mm/mm) this is mentioned in the (Figures 19-23) in regards to the (Figures 19 and 20) show that the two discs intervertebral (D3, D4) are most damaged that is disc degeneration often begins after a phase of asymptomatic dehydration by cracks, tears two annulus (D3, D4), the two cores (N3, N4) can then along these cracks migrate into the thickness of two rings (D3, D4) and cause acute or chronic back pain, If the two cores (N3 , N4) move further through two rings (D3, D4), the two cores may project to the posterior face of

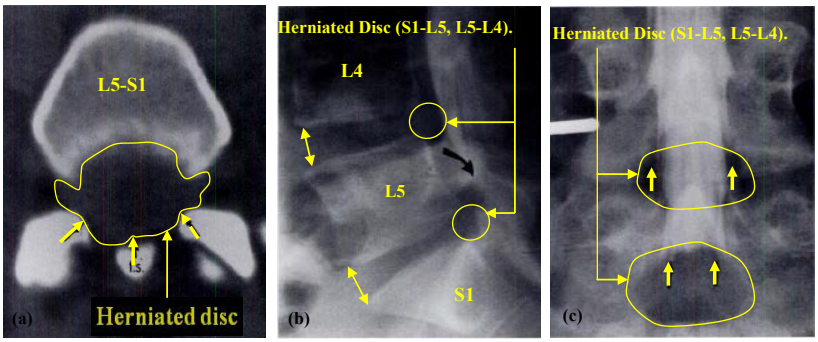

Figure 36: Standard profile of the lumbar sacral spine radiograph of a boy of 16 years showing: (a) disc pinching (L5-S1, L5-L4), (b) TDM lumbosacral of spine axial section showing a herniated disc median (L5-S1) posterolateral left, (c) lumbosacral MRI showing a posterior disc herniation (L5-S1), progression disc level (L5-L4), (D) MRI axial section showing a posterolateral disc left hernia (S1-L5) [47].

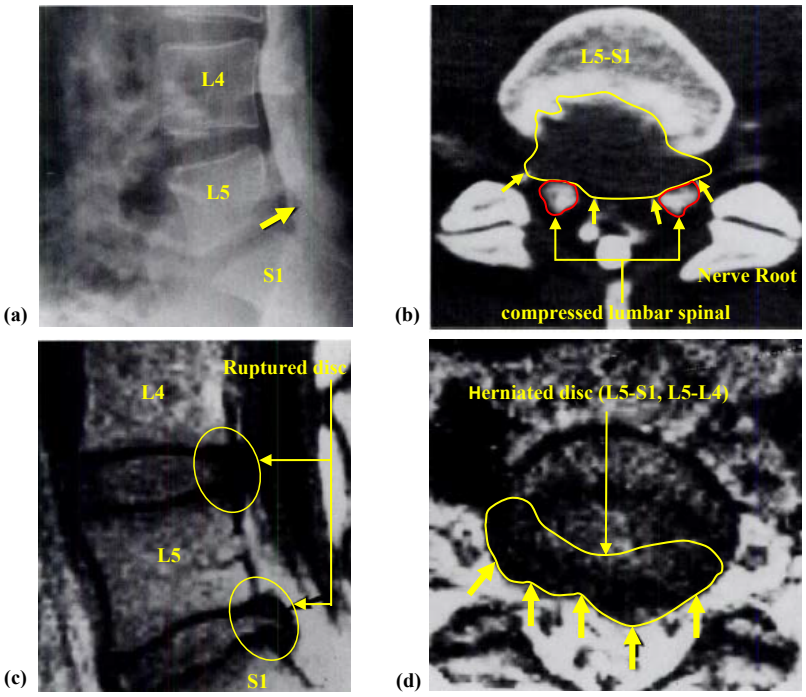

Figure 37: Standard profile of the lumbar sacral spine radiograph of a boy of 16 years showing: (a) disc pinching (L5-S1, L5-L4), (b) TDM lumbosacral of spine axial section showing a herniated disc median (L5-S1) posterolateral left, (c) lumbosacral MRI showing a posterior disc herniation (L5-S1), progression disc level (L5-L4), (D) MRI axial section showing a posterolateral disc left hernia (S1-L5) [47].

the disc while forming a herniated disc (Figures 36 and 37), This hernia can through a complete rupture of the annulus, migrate laterally into the vertebral canal, or up or down, and even exclude leaving the disc, herniated disc that can come compress "stuck "one or more nerve roots near the disk, it is the cause of symptoms" sciatica "pain when the seat back of the thigh or" cruralgie "when pain seat in front of the thigh. This justifies that the distance between the load which is the point of application of the load and the axis of the spine plays an important role in the increase of stresses in the intervertebral discs.

Conclusion

In sum, we concluded the case of posterior loading, a 300 mm lever with a 150 N montreent force maximum normal stresses of Von Mises in four intervertebral discs (D1, D2, D3, D4) and are equal to (3.1168 MPa, 3.1615 MPa, 7.5682 MPa, 6.6882 MPa). Figures 19-22 clearly shows that the amount of elastic deformation is highest in the four intervertebral discs (D1, D2, D3, D4) which are equal to (0.82801 mm/mm 0.7792 mm/mm 1.9066 mm/mm 1.6041 mm/mm) This justifies that the distance between the load which is the point of application of the load and the axis of the spine plays a very important role in increasing the solitation of the latter.

Acknowledgements

The authors extend their appreciation to the Director of Scientific Research at LaBPS for funding the work through the Biomechanics Research Group.

References

1. Cheng H (2007) A finite element study of the biomechanical behavior of the nonlinear ligamentous thoracic and lumbar spine.
2. Saal JA (1996) Natural history and nonoperative treatment of lumbar disc herniation. Spine 21: 2S-9S.

3. Fardon DF, Milette PC (2001) Nomenclature and classification of lumbar disc pathology. Recommendations of the Combined task Forces of the North American Spine Society, American Society of Spine Radiology, and American Society of Neuroradiology. Spine 26: E93-E113.

4. Harris W, Fleming J, Gertzbein S (2003) Back Pain: The workplace safety and insurance appeals tribunal.

5. Wilder DG, Pope MH, Frymoyer JW (1998) The biomechanics of lumbar disc herniation and the effect of overload and instability. J Spinal Disord 1: 16-32.

6. Miller JA, Schmatz C, Schultz AB (1998) Lumbar disc degeneration: correlation with age, sex, and spine level in 600 autopsy specimens. Spine 13: 173-178.

7. Matsui H, Kanamori M, Ishihara H (1998) Familial predisposition for lumbar degenerative disc disease. A case-control study. Spine 23: 1029-1034.

8. Tsuji H, Hirano N, Ohshima H (1993) Structural variation of the anterior and posterior anulus fibrosus in the development of human lumbar intervertebral disc. A risk factor for intervertebral disc rupture. Spine 18: 204-210.

9. Taylor TK, Akeson WH (1971) Intervertebral disc prolapse: A review of morphologic and biochemic knowledge concerning the nature of prolapse. Clin Orthop Relat Res 76: 54-79.

10. Gertzbein SD, Hollopeter MR (2002) Disc herniation after lumbar fusion. Spine 27: E373-376.

11. Hernie Discale Lombaire, Service de Chirurgie orthopédique et Traumatologique, Hôpital Beaujon.

12. Kassab M, Centre Avicenne Médical, 2 Av Tahar Sfar, 2092, El Manar 2, Tunis, Tunisie.

13. White Iii AA, Panjabi MM (1990) Clinical biomechanics of the spine.

14. Champain SM (2008) Corrélations entre les parametres biomecaniques du rachis et les indices cliniques pour l'analyse quantitative des pathologies du rachis lombaire et de leur traitement chirurgical, Enam, Paris.

15. Francois L (1997) Biomécanique Et Ostéosynthèse Du Rachis Ensm-Lbm Conférences D'enseignement De La Sofcot.

16. Starmans FJ, Steen WH, Bosman F (1993) A three-dimensional, finite-element analysis of bone around dental implants in an edentulous human mandible. Arch Oral Biol 38: 491-496.

17. Ibarz E, Más Y, Mateo J, Lobo-Escolar A, Herrera A, et al. (2013) Instability of the lumbar spine due to disc degeneration. a finite element simulation. Advances In Bioscience and Biotechnology 4: 548-556.

18. Mingzhi S, Zhen Z, Ming L, Junwei Z, Chao D, et al. (2014) Four lateral mass screw fixation techniques in lower cervical spine following laminectomy. A finite Element Analysis Study Of Stress Distribution. Biomed Eng 13: 115.

19. Steven A, Rundell, MS, Jorge E, Isaza, Steven M, et al. (2011) Biomechanical Evaluation Of A Spherical Lumbar Interbody Device At Varying Levels Of Subsidence. Exponent, inc, philadelphia, pa, sas j 5: 16-25.

20. Vijay GK, Ankit M, Jayant BS, Faizan A, Ali, et al. (2007) Anatomic facet replacement system (AFRS) restoration of lumbar segment mechanics to intact. A finite element study and in vitro cadaver investigation. SAS J 1: 46-54.

21. Holekamp S, Goel V, Hiroshi K, Janet, Nabil E (2007) Optimal Intervertebral Sealant Properties for the Lumbar Spinal Disc. A Finite-Element Study. SAS J. Spring 1: 68-73.

22. Castellvi AE, Huang H, Vestgaarden Tov, Saigal S, Clabeaux DH, et al. (2007) Stress reduction in adjacent level discs via dynamic instrumentation. a finite element analysis. SAS J. Spring 1: 74-81.

23. López E, Elena I, Herrera A, Mateo J, Lobo-Escolar A, et al. (2014) Probability of osteoporotic vertebral fractures assessment based on dxa measurements and finite element simulation. Advances in Bioscience and Biotechnology 5: 527-545.

24. Kiapour A, Kiapour AM, Kodigudla M, Hill GM, Mishra S, et al. (2012) A biomechanical finite element study of subsidence and migration tendencies in stand-alone fusion procedures. Comparison of an in situ expandable device with a rigid device. J Spine 1: 2165-7939.

25. Zheng SN, Yao QQ, Wang LM, Hu WH, Wei B, et al. (2013) Biomechanical effects of semi constrained integrated artificial discs on zygapophysial joints of implanted lumbar segments. Experimental and Therapeutic Medicine 6: 1423-1430.

26. Byun DH, Shin DA, Kim JM, Kim SH, Kim HI (2012) Finite Element Analysis of the Biomechanical Effect of Coflex™ on the Lumbar Spine. laboratory investigation. Korean J Spine 9: 131-136.

27. Lan Ch, Kuo ChS, Chen ChH, Hu HT (2013) Finite element analysis of biomechanical behavior of whole thoraco-lumbar spine with ligamentous effect. The Changhua Journal of Medicine 11: 26-41.

28. Natarajan RN, Andersson GBJ (1997) Modeling the annular incision in a herniated lumbar intervertebral disc to study its effect on disc stability. Comput Struct 64: 1291-7.

29. Pitzen T, Geisler FH, Matthis D, Storz HM, Pedersen K, et al. (2001) The influence of cancellous bone density on load sharing in human lumbar spine: a comparison between an intact and a surgically altered motion segment. Eur Spine J 10: 23-9.

30. Polikeit A (2002) Finite element analysis of the lumbar spine: Clinical application. Inaugural dissertation. University of Bern.

31. Denozi´Ere G (2004) Numerical modeling of a ligamentous lumber motion segment, M.S. thesis, Department of Mechanical Engineering. Georgia Institute of Technology. Georgia. USA.

32. Shin G (2005) Viscoelastic responses of the lumbar spine during prolonged stooping dissertation, NCSU, USA.

33. Sairyo K, Goel VK, Masuda A, Vishnubhotla S, Faizan A, et al. (2006) Three-dimensional finite element analysis of the pediatric lumbar spine. Eur Spine J 15: 923-9.

34. Rohlmann A, Burra Nk, Zander T, Bergmann G (2007) Comparison of the effects of bilateral posterior dynamic and rigid fixation devices on the loads in the lumbar spine. Eur Spine J 16: 1223-31.

35. Wilke Hj, Neef P, Caimi M, Hoogland T, Claes Le (1999) New intradiscal pressure measurements in vivo during daily activities. Spine 24: 755-62.

36. Smit T, Odgaard A, Schneider E (1997) Structure and function of vertebral trabecular bone. Spine 22: 2823-2833.

37. Sharma M, Langrana Na, Rodriguez J (1995) Role of ligaments and facets in lumbar spinal stability. Spine 20: 887-900.

38. Lee K, Teo E (2004) Effects of laminectomy and facetectomy on the stability of the lumbar motion segment. Med Eng Phys 26: 183-92.

39. Rohlmann A, Zander T, Schmidt H, Wilke Hj, Bergmann G (2006) Analysis of the influence of disc degeneration on the mechanical behaviour of a lumbar motion segment using the finite element method. J Biomech 39: 2484-90.

40. Ng Hw, Teo Ec (2001) Nonlinear finite-element analysis of the lower cervical spine (C4–C6) under axial loading. J Spine Disord 14: 201-10.

41. Ng HW, Teo ECh, Zhang QH (2004) Influence of laminotomies and laminectomies on cervical spine biomechanics under combined flexion-extension. J of Applied Biomechanics 20: 243-259.

42. Gong Z, Chen Z, Feng Z, Cao Y, Jiang Ch, et al. (2014) Finite element analysis of 3 posterior fixation techniques in the lumbar spine. Feature Article 37: E441-E448.

43. Kim HJ, Tak Kang K, Chang BS, Lee ChK, Kim JW, et al. (2014) Biomechanical analysis of fusion segment rigidity upon stress at both the fusion and adjacent segments-a comparison between unilateral and bilateral pedicle screw fixation. Yonsei Med J 55: 1386-1394.

44. Goel VK, Kiapour A, Faizan A, Krishna M, Tai F (2006) Finite Element Study of Matched Paired Posterior Disc Implant and Dynamic Stabilizer (360° Motion Preservation System). SAS J 1: 55-61.

45. Tang Sh, Meng Xueying (2010) Does Disc Space Height of Fused Segment Affect Adjacent Degeneration In ALIF. A Finite Element Study. J Turkish Neurosurgery 3: 296-303.

46. Kim KT, Lee SH, Suk KS, Lee JH, Jeong BO (2010) Biomechanical Changes of the Lumbar Segment After Total Disc Replacement: Charite®, Prodisc® and Maverick® Using Finite Element Model Study. J Korean Neurosurg Soc 47: 446-453.

47. Agarwal A, Agarwal AK, Goel VK (2013) The endplate morphology changes with change in biomechanical environment following discectomy. International J of Clin Med 4: 8-17.

48. Zhong ZCh, Wei SH, Wang JP, Kol (2006) Finite element analysis of the

lumbar spine with a new cage using a topology optimization metod. Medical Engineering & Physics 28: 90-98.

49. Goto K, Tajima N, Chosa E, Kol (2002) Mechanical analysis of the lumbar vertebrae in a three-dimensional finite element method model in which intradiscal pressure in the nucleus pulposus was used to establish the model. J Orthop Sci 243-246.

50. Rodriguez DP, Poussaint TY (2010) Imaging of Back Pain in Children 31: 787-802.

51. Lukhele M, Mayet Z, Dube B (2011) Lumbar disc herniation in a 9-year-old child 10: 3.

52. Erwin MJC, Emile AMB, Biene WW, Johannes SHV (2014) Thoraco-Lumbar junction disc herniationand tight filum: a unique coieunration.

53. Afshani E, Jerald P, Kuhn (1991) Common Causes of Low Back Pain in Children.

Citation: Zahaf S, Mansouri B, Belarbi A, Azari Z (2016) The Effect of the Posterior Loading on the Spine of a School Child. Adv Cancer Prev 1: 112. doi: 10.4172/2472-0429.1000112